

Article

Not peer-reviewed version

An Overview of Design Techniques for Two-Dimensional Leaky-Wave Antennas

[Edoardo Negri](#) , [Walter Fuscaldo](#) , [Paolo Burghignoli](#) , [And Alessandro Galli](#) *

Posted Date: 3 January 2025

doi: 10.20944/preprints202501.0142.v1

Keywords: Leaky-Wave Antennas; Numerical Methods; Fabry-Perot Cavity Antennas; Radially Periodic Leaky-Wave Antennas; Metasurfaces







Preprints.org is a free multidisciplinary platform providing preprint service that is dedicated to making early versions of research outputs permanently available and citable. Preprints posted at Preprints.org appear in Web of Science, Crossref, Google Scholar, Scilit, Europe PMC.

Copyright: This open access article is published under a Creative Commons CC BY 4.0 license, which permit the free download, distribution, and reuse, provided that the author and preprint are cited in any reuse.

Article

An Overview of Design Techniques for Two-Dimensional Leaky-Wave Antennas

Edoardo Negri ^{1,2} , Walter Fuscaldo ² , Paolo Burghignoli ¹  and Alessandro Galli ^{1,*} 

¹ Department of Information Engineering, Electronics and Telecommunications, Sapienza University of Rome, 00184 Rome, Italy

² Istituto per la Microelettronica e Microsistemi, Consiglio Nazionale delle Ricerche, 00133 Rome, Italy

* Correspondence: alessandro.galli@uniroma1.it

Abstract: Two-dimensional leaky-wave antennas offer effective, compact, single-feeder, easy-to-fabricate solutions to the longstanding problem of realizing a simultaneously directive and low-profile radiating device. These traveling-wave antennas have been thus proposed as wideband, reconfigurable, or frequency-scanning radiating structures in different application contexts, ranging from the microwave to terahertz frequency range. These diverse contexts call for a comprehensive guide for characterizing and designing two-dimensional leaky-wave antennas. In this work, a review of numerical techniques for the analysis of either quasi-uniform or radially periodic leaky-wave antennas is proposed. Theoretical results are corroborated through full-wave simulations of realistic three-dimensional models of the designed devices, thus demonstrating the effectiveness of the proposed methods.

Keywords: leaky-wave antennas; numerical methods; fabry–perot cavity antennas; radially periodic leaky-wave antennas; metasurfaces

1. Introduction

Leaky-wave antennas (LWAs) are radiating devices constituted by waveguiding structures which allow for continuous power radiation while propagating along their length [1–3]. Although the working principle is rather intuitive, the design of radiating devices by partially open waveguides found its mathematical and physical rigorous foundation only in the '50s thanks to the famous work of N. Marcuvitz [4]. This paper, together with the works of T. Tamir and A. A. Oliner [5,6], had an important impact on the development of LWAs: thanks to an efficient and elegant theory, rather simple analytical procedures were outlined for designing such radiating devices, in a period when the computational resources were very limited.

It is well-known that this kind of radiating devices shows many advantages since LWAs are simple and low-cost solutions able to generate highly directive beams pointing at almost arbitrary angles [7]. Moreover, they show a reconfigurability feature in terms of pointing angles since their beam naturally scans with frequency [8] or, if a fixed frequency is desired, they are able to scan electronically by incorporating tunable elements into the design, such as varactor diodes [9], ferrites [10], microelectromechanical systems [11] based on micromachining technologies [12], graphene [13,14], or liquid crystals [15].

The main critical aspects of LWAs are typically related to the following trade-offs: pattern fractional bandwidth vs. directivity (leaky-wave antennas are usually highly directive but show a narrow bandwidth), reconfigurability vs. complexity (the higher is the desired reconfigurability feature at fixed frequency, the more complex is the device architecture), and radiation efficiency vs. aperture size (a large radiating aperture is needed to achieve a highly directive antenna) [2]. Fortunately, in recent years, different solutions have been proposed to overcome these issues. For instance, in order to enhance the figure of merit given by the product of directivity and bandwidth, Fabry–Perot cavity antennas (FPCAs) with a thick partially reflecting sheet (PRS) [16,17] or high truncation effects [18,19]

have been proposed and studied through different techniques. As concerns, instead, reconfigurable leaky-wave antennas, different, easy-to-implement technological solutions have been addressed in the recent years from the microwave to the terahertz frequency ranges [20–22]. Moreover, the longstanding problem of designing directive LWAs through compact devices has been solved by exploiting tapering techniques [23,24].

The effectiveness and the importance of LWAs from both a theoretical and a practical viewpoint are thus clear. However, a paper reviewing simple numerical techniques for characterizing and designing LWAs is still missing. This work aims to fill this gap by describing, step by step, the design workflow of uniform and radially periodic two-dimensional (2-D) LWAs which represent the common architectures of more sophisticated solutions, such as holographic [25] and modulated surface antennas [26–29], or even near-field focusing devices [30–33].

The manuscript is organized as follows. In Section 2, an established classification of LWAs is presented, highlighting the need for various approaches to analyze different kinds of these radiators. In Sections 3 and 4, the numerical techniques for the analysis and design of uniform and radially periodic 2-D LWAs are presented, respectively. Conclusions are finally drawn in Section 5.

2. Classification of Leaky-Wave Antennas

In this Section, a widely accepted [1,8] classification of LWAs is provided with the aim of introducing the different working principles and radiating features of the devices discussed in this work.

The first distinction among LWAs is related to the *geometry* of the radiating device. In particular, one-dimensional (1-D) and 2-D LWAs are distinguished depending on whether the guiding structure is mainly linear or planar, respectively. In other terms, a principal fixed direction of propagation can be easily identified in 1-D LWAs (see Figure 1a), whereas 2-D LWAs are in general radial devices commonly fed in the center, which are characterized by a partially guided wave propagating along a plane (see Figure 1b). This aspect affects the radiation features of the device since a 1-D structure is in general able to produce *fan beams*, whereas a 2-D structure is mainly used for *pencil beams* or fully *conical beams* depending on the frequency [8].

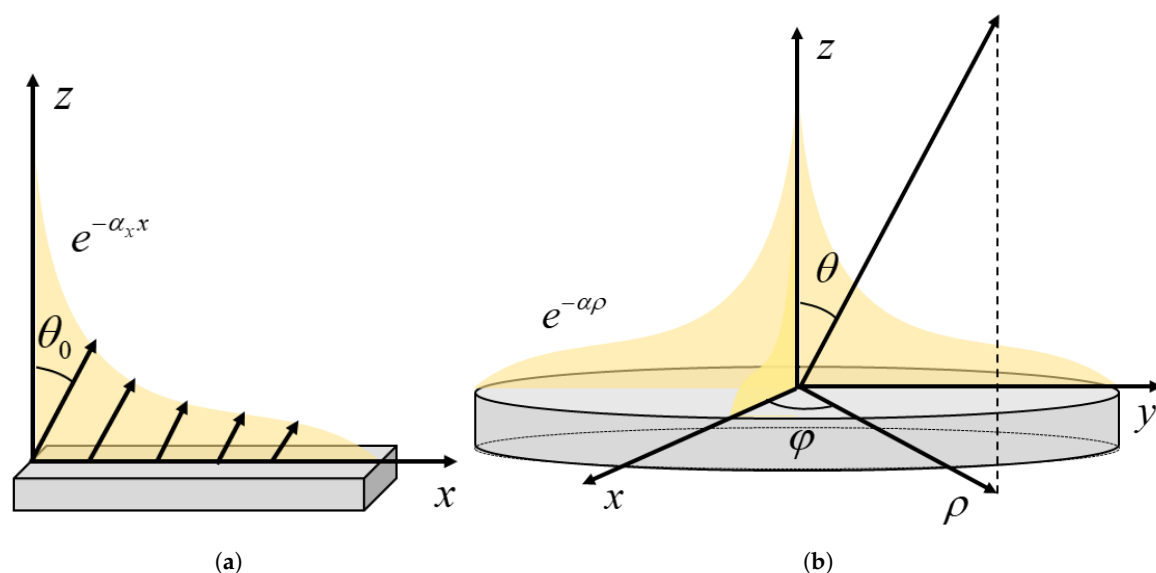


Figure 1. (a) Pictorial representation of a 1-D LWA. The electromagnetic field is partially guided in the x direction in the gray structure. Due to radiation, the amount of transmitted power has an exponential decay related to the leakage constant α_x , generating a far-field radiation pattern pointing in the θ_0 direction. (b) Schematic view of a 2-D LWA. As in (a), the electromagnetic field is partially guided in the gray structure, undergoing to an exponential decay of the transported power related to the leakage constant α in the radial direction.

The other classification concept, which affects the scanning behavior of the antenna, is related to the *working principle* of the device and it allows us to define uniform, quasi-uniform, and periodic LWAs. When the cross section of the radiator remains constant along the direction of propagation, the structure is usually referred to as *1-D uniform LWA*. A typical historical example consists in a rectangular waveguide with a longitudinal slit (see Figure 2a) which allows the power to leak while propagating [34–36]. The radiation is usually related to the perturbation of the fundamental guided mode, which is in general a *fast wave*. In the *transmission* mode, 1-D LWAs are commonly fed from one side of the input waveguide launching the traveling leaky wave. By properly varying the working frequency, the main beam is scanned from nearly broadside to nearly endfire, with some intrinsic problems for the generation of a beam exactly at broadside or endfire [8]. In other cases, a bidirectional feeding of the waveguiding structure is also possible, with the same leaky wave propagating in opposite directions from a central feed [8].

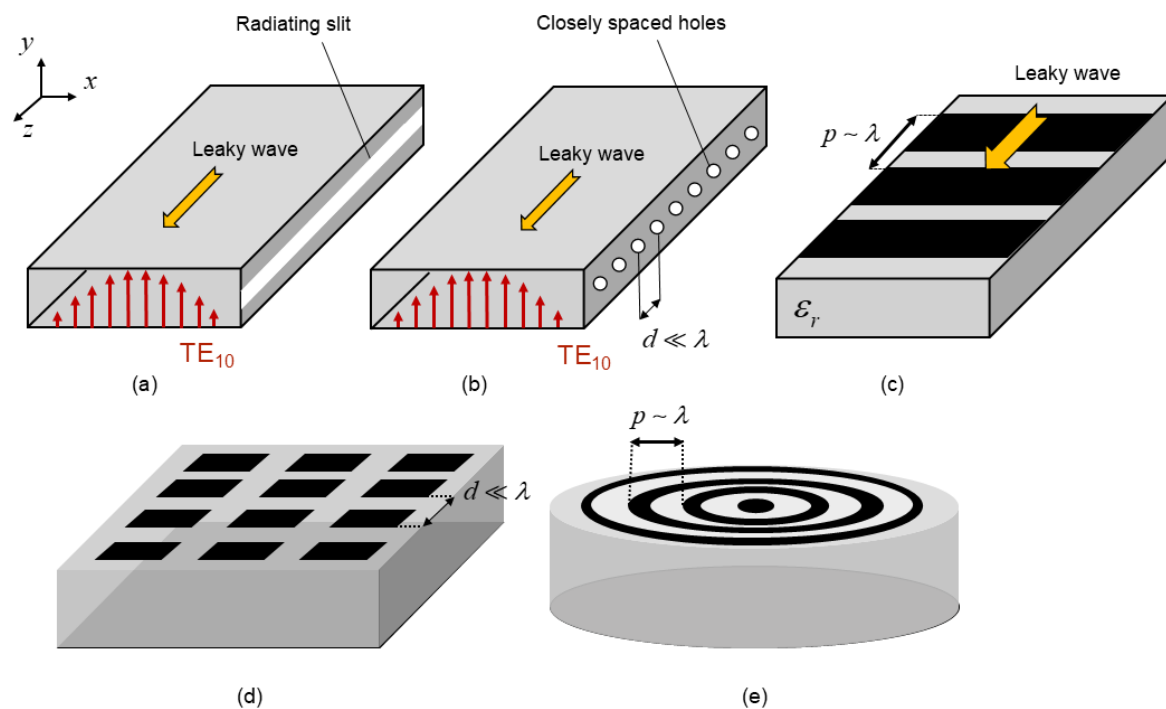


Figure 2. Pictorial representation of (a) a slitted rectangular waveguide (uniform 1-D LWA), (b) a rectangular waveguide with closely spaced holes (quasi-uniform 1-D LWA), (c) a grounded dielectric slab (GDS) with relative permittivity ϵ_r and with a metal strip grating supporting periodicity $p \sim \lambda$ on top (1-D periodic LWA), (d) a GDS supporting a 2-D periodic screen with periodicity $d \ll \lambda$ (quasi-uniform 2-D LWA), and (e) a GDS supporting annular concentric microstrip rings (radially periodic 2-D LWA).

When there is a periodic modulation of the geometry on the longitudinal direction of the radiating structure with a periodicity dimension d much lower than the operating wavelength λ , the device is referred to as *1-D quasi-uniform LWA*. The radiation properties of this kind of antennas are similar to those of 1-D uniform LWAs since both of them work with only the fundamental mode in propagation. The performance, however, can significantly be improved with respect to the uniform case by properly engineering the periodic modulation. For instance, the idea proposed in [37] to reduce the leakage rate and achieve a more directive antenna with respect to the uniform, slotted, rectangular waveguide, was to consider closely placed holes rather than a continuous, longitudinal slit responsible of cutting the current lines on the metal walls of the guide (see Figure 2b).

When there is a periodic modulation of the geometry along the longitudinal direction of the radiating structure with a periodicity dimension p approximately larger than half of the operating wavelength λ , the device is referred to as *1-D periodic LWA*. The difference with respect to the 1-D quasi-uniform LWA is given by their working principle. While in the quasi-uniform case there is

only the fundamental, basically *fast* mode in propagation, in 1-D *periodic* LWAs the guided wave is represented by an infinite number of *Floquet modes* (or *space harmonics*) due to the larger periodicity. A typical example of 1-D periodic LWAs is a dielectric waveguide or a microstrip that is loaded by perturbations with periodicity comparable to the wavelength [38] (see Figure 2c). As is common in this kind of structures, the fundamental Floquet mode is usually *slow*. For this reason, the LWA is typically designed so that the $n = -1$ harmonic is fast in order to let the device radiate. The main advantage of 1-D periodic LWAs with respect to the abovementioned classes is the possibility to scan from the backward to the forward quadrant. It is however worthwhile to point out that the antenna performance strongly degrades when the main beam approaches broadside. This issue, due to the presence of an *open stopband*, has been strongly analyzed, and actions to mitigate its adverse effects have been studied (see, e.g., [29,39–41]).

The definition of LWAs based on the working principle of 1-D structures can be extended to the 2-D case. Two-dimensional *uniform* and *quasi-uniform* LWAs are indeed 2-D partially open waveguiding structures able to support a *cylindrical leaky wave* which radially propagates outward from the central source [42]. This kind of LWA, typically by varying the frequency, can produce a directive pencil beam at broadside or a conical beam with the cone axis corresponding to the vertical axis. Interestingly, by considering an array feeding scheme, a directive pencil beam can be achieved off broadside [43], even with a circular polarization if a proper polarization-conversion metasurface is employed [44–46]. As for their 1-D counterpart, the radiation features of 2-D uniform and *quasi-uniform* LWAs are commonly related to the fundamental leaky mode, which is a *fast wave*. One of the most important example of 2-D uniform LWAs is a grounded dielectric slab (GDS) with a PRS on top, constituting an FPCA (see Figure 2d) [47].

Similarly to the distinction among 1-D *periodic* and *uniform* or *quasi-uniform* LWAs, it is possible to define a 2-D *periodic leaky-wave antenna* when a 2-D partially open waveguiding structure presents a periodic modulation capable of propagating higher-order Floquet modes. If the periodicity occurs only in one dimension, which is the common case study, the radiating device is referred to as *1-D periodic 2-D LWA*. A typical example in this context, which corresponds to the structure analyzed in this work, is the case of an annular metal strip grating printed on top of a GDS (see, e.g., [48]) where the periodicity is present only in the radial direction (see Figure 2e). If the periodicity occurs in two directions, as in the case of a metal-patch array printed on a GDS studied in [49], the radiating device is referred to as *2-D periodic 2-D LWA*.

This work deals with the numerical methods and the design rules which can be efficiently used for characterizing 2-D uniform and quasi-uniform LWAs (FPCAs) and 1-D periodic 2-D LWAs. These approaches can profitably be exploited also for the design of their 1-D counterparts [31,50].

3. Fabry–Perot Cavity Antennas

This Section deals with the design of FPCAs. While the theoretical working principles and design workflow for these radiating devices are presented in Section 3.1, the numerical techniques needed for describing such FPCAs are reported in Sections 3.2 and 3.3. The possible realizations of a feeder for such devices are then reported in Section 3.4 as well as the implementation of an efficient and fast full-wave simulation of FPCAs is shown in Section 3.5.

3.1. Theoretical Background

Fabry–Perot cavity antennas are constituted by a grounded dielectric slab with a partially reflecting sheet on top. These devices are usually fed through dipole-like sources in the middle (see Figure 3(a)). If a vertical electric dipole (VED) —which can be easily implemented through a coaxial cable [51,52]— or a vertical magnetic dipole (VMD) —commonly realized through a loop antenna [53,54]— is exploited, a cylindrical leaky wave with a pure transverse magnetic (TM) or electric (TE) polarization is excited, thus generating an omnidirectional conical beam. However, radiation at broadside is prevented in this case by the null enforced by the source geometry [47]. With the aim of achieving a broadside pencil beam, a horizontal magnetic dipole (HMD) —commonly implemented through a slot on the ground

plane excited by a microstrip [7] or a rectangular waveguide [55–57]— or a horizontal electric dipole (HED) —typically realized through a L-probe, bent coaxial feed [58,59]— has to be employed. Such sources excite both TE and TM cylindrical leaky waves [42] and, thus, some difficulties in producing omnidirectional conical beams may arise due to possible TE–TM disequalization [47].

Once the feeder has been properly chosen, physically implemented, and matched (as discussed in the following Section 3.4), the goal is to properly design the FPCA to achieve the desired performance in terms of directivity, pointing angle, working frequency, bandwidth, and efficiency. This objective can be achieved by simultaneously designing the PRS with the GDS characteristics, viz. the cavity height h , the lateral dimension L , and the dielectric-filling permittivity ϵ_r (see Figure 3a). On the one hand, the beam angle mainly depends on the electrical thickness of the cavity [60]. On the other hand, the reflectivity of the PRS controls how much power leaks during propagation. For this reason, the beamwidth mainly depends on PRS design [61]. These intuitive physical concepts can be rigorously described through the *leaky-wave theory* [47] or the *reciprocity approach* [62], obtaining, in both cases, closed-form design equations for FPCAs.

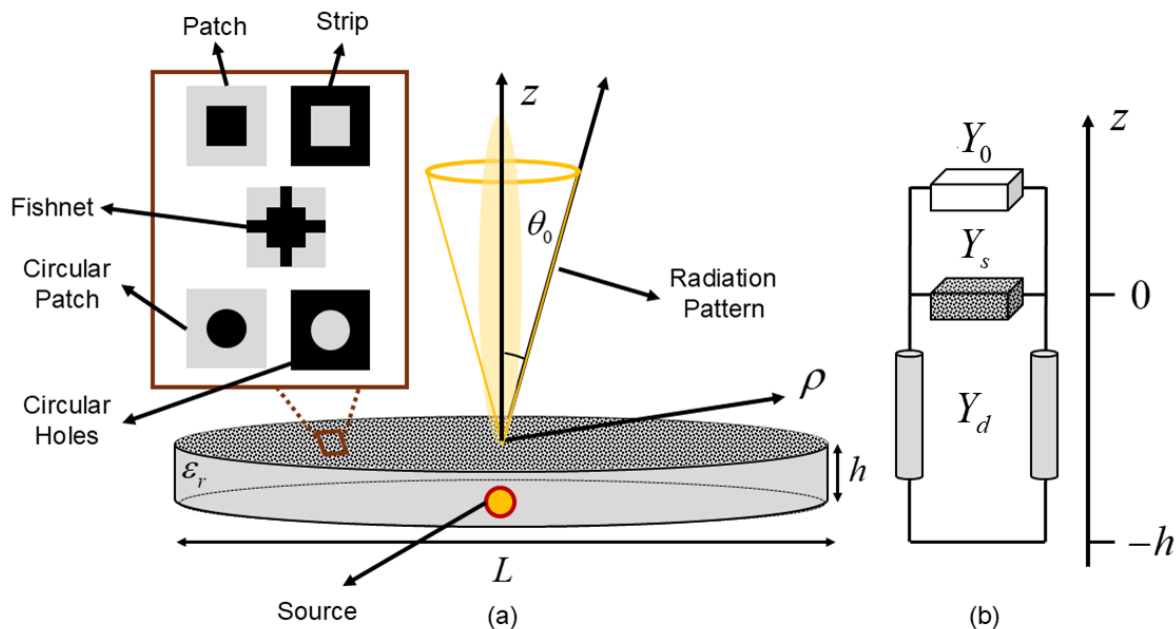


Figure 3. (a) Schematic representation of an FPCA (constituted by a grounded dielectric slab—in gray—with a PRS on top), of its source (realized through dipole-like feeders), and its far-field radiation pattern (which can be a broadside pencil beam or a scanned conical beam). The red box on the left represents the possible implementations of the PRS unit cells through simple isotropic metasurfaces based on metallic lattices (black regions) printed on top of the dielectric slab (gray areas). (b) Transverse equivalent network of the FPCA. Y_0 and Y_d represent the characteristic admittances of the free space and the dielectric constituting the cavity, respectively, and Y_s is the equivalent surface impedance of the PRS.

The first parameter which can be easily chosen is the minimum lateral dimension L of the FPCA (see Figure 3a). Such a parameter has to be designed to maintain the radiating features of an infinite structure almost unchanged when the real antenna is implemented and, thus, to achieve high radiation efficiency (assuming a lossless structure). In other terms, this means that L has to be designed to avoid significant edge effects. The design goal in order to achieve a very high aperture efficiency is thus to reach the lateral aperture with power as low as possible or, in other terms, to let almost all the transmitted power radiate before reaching the FPCA lateral boundaries. In *lossless* FPCAs, the radiation efficiency is given by [1,8]:

$$\eta_L = 1 - e^{-\alpha L} \quad (1)$$

A simple design equation for L is thus found for a desired value of the aperture efficiency (a typical minimum lower bound is set at $\eta_L = 90\%$ [47]):

$$L = -\frac{\ln(1 - \eta_L)}{\alpha} \quad (2)$$

It is thus clear the importance of accurately evaluating the leaky attenuation constant α for the correct design of the device. Such parameter not only affects the aperture efficiency, but also the beamwidth, the directivity, and the fractional bandwidth (FBW).

On the other hand, the leaky phase constant β mainly determines the pointing angle of the device at a given frequency. For this reason, in general, the correct evaluation of the leaky wavenumber $k_\rho = \beta - j\alpha$ —with β and α being the leaky phase and attenuation constants, respectively—plays a fundamental role. This procedure is addressed through the *transverse resonance technique* which is deeply discussed in the next subsection. This method requires the representation of the FPCA through a transverse equivalent network (see Figure 3b): the GDS is considered as a transmission-line section whose dimension and characteristic impedance depends on the cavity height, the considered polarization, and the dielectric permittivity of the material (assuming for simplicity $\mu_r = 1$); the PRS, if lossless (the lossy case is a natural evolution of this analysis and it is discussed in [63]) is commonly well represented through a purely imaginary impedance sheet $Z_s = jX_s$ [64,65] (see, e.g., the inset on the left in Figure 3a,b).

In the leaky-wave perspective, the radiation features of the FPCAs are known once the leaky-wave wavenumber is correctly evaluated. By assuming that the feeder launches an omnidirectional cylindrical leaky wave with small attenuation constant $\alpha \ll k_0$ (where k_0 is the vacuum wavenumber), the latter provides the main contribution to the field on the antenna aperture plane at $z = 0$ (see Figure 3a) [5,6]. These cylindrical leaky waves are known in closed formulas (reported for the first time in [42]) and they can be used to evaluate the far-field radiation pattern through a simple Fourier transform, thus obtaining (assuming an infinite aperture):

$$\text{SF}(\theta) = \frac{4|k_\rho|^2}{|k_\rho^2 - k_0^2 \sin^2 \theta|^2} \quad (3)$$

where SF stands for space factor.

From the far-field radiation pattern in (3), one can easily retrieve important design relations [42]. For instance, the maximum value of SF for different θ angles is obtained by minimizing the denominator in (3). It is thus clear that the pointing angle for the FPCA is given by:

$$\theta_0 = \arcsin \left[\sqrt{\left(\frac{\beta}{k_0}\right)^2 - \left(\frac{\alpha}{k_0}\right)^2} \right] \quad (4)$$

Since $\alpha \ll k_0$ in order to have a dominant leaky-wave contribution on the leaky-wave aperture [5,6], Equation (4) reveals that β mainly determines the pointing angle θ_0 . Starting from Equation (3), one can also easily derive the half-power beamwidth (HPBW) $\Delta\theta$ as [47]:

$$\Delta\theta = 2 \frac{\alpha}{k_0} \sec \theta_0 \quad (5)$$

Also Equation (5) reveals an important result. The beamwidth, which is strictly related to the directivity, mainly depends on the attenuation constant α . The lower is α , the narrower is the beamwidth and, in turn, the pattern is peaked at the pointing-angle direction. Therefore, the more the PRS is reflective and, in turn, the lower is α (since the PRS reactance controls the amount of power which leaks out), the more directive is the antenna. This relation has been expressed in a closed formula for an FPCA radiating at broadside as [47]:

$$D \simeq \frac{k_0^2 \pi^2}{8\alpha^2} \quad (6)$$

It is worthwhile to point out that the attenuation constant is also strictly related to the bandwidth. In particular, it has been shown in [66] that, when broadside radiation is considered, the fractional bandwidth (FBW) —defined as the frequency band, normalized with respect to the central frequency, for which the power density at broadside drops less than one half (3 dB) [62]— can be computed as [47]:

$$\text{FBW} = \frac{2\alpha^2}{k_0^2 \epsilon_r} \quad (7)$$

By observing Equations (6) and (7), an evident *trade-off* between directivity and fractional bandwidth appears. The figure of merit (FoM) given by the product $D \cdot \text{FBW}$ for an FPCA based on a single thin PRS is constant and equal to:

$$\text{FoM} = D \cdot \text{FBW} \simeq \frac{2.47}{\epsilon_r} \quad (8)$$

It is thus clear that low-permittivity and low-loss materials are the best choice for the design of directive antennas.

With these formulas in mind, one can easily find three different working conditions for FPCAs depending on the mutual comparison between β and α . When $\beta < \alpha$, the FPCA radiates at broadside [66] in the so-called *reactive* region. A deep analysis of FPCAs radiating in this frequency range has been presented in [67]. The condition $\beta \simeq \alpha$ provides, instead, the best working point to maximize the radiated power at broadside [66]. In this context, a broadside pencil beam is produced by the FPCA with a beamwidth which depends on the X_s or, equally, to the α value. Finally, by increasing the frequency, the condition $\beta > \alpha$ is reached. In this working region, FPCAs generate a scanning conical beam whose pointing angle mainly depends on the β value through (4) and the beamwidth on the α value as (5) (and, in turn, on the X_s value). These aspects, along with additional design formulas, are rigorously addressed by exploiting the *transverse resonance technique* discussed in the following subsection.

3.2. Evaluation of the Dispersion Curves

The standard procedure for retrieving the eigenvalues in waveguiding structures derives from the solution of Maxwell's equations in any homogeneous region of the domain of interest and the application of the boundary conditions [68]. A nontrivial solution is then obtained by discretizing the problem, thus reducing it to a linear algebraic system, and enforcing the determinant of the coefficient matrix to be equal to zero. The complex roots of the resulting determinantal equation—which is commonly referred to as *dispersion equation*— are the desired eigenvalues. This approach allows for expressing any solution of the problem with its eigenvalue (the mode of the waveguide) and eigenfunction (the modal field) up to a multiplicative constant which depends on the excitation. This procedure, however, could be lengthy for devices with different media and complicated structures. Since, in the leaky-wave perspective, we are usually interested only in the evaluation of the eigenvalues, a faster approach is given by the *transverse resonance technique* [69]. It is indeed well known [70] that the eigenvalues of a waveguide problem correspond to pole singularities of an appropriate characteristic Green's function in the k_z complex plane, which represents the voltage (or current) in a transmission line along one of the transverse directions of the waveguide [5,6]. Within this network formalism, the pole singularities correspond to resonances of the transverse equivalent network (TEN) model, which can be conveniently calculated using analytical and numerical methods.

Since FPCAs are constituted by a grounded dielectric slab with a PRS on top, their TEN is formed by a transmission-line segment—with characteristic admittance Y_d and transverse number $k_{zd} = \sqrt{k_0^2 \epsilon_r - k_p^2}$ — terminated, on one side, on the equivalent sheet admittance of the PRS Y_s , and, on the other side, on a short circuit representing the ground plane (see Figure 3b). The term PRS refers in general to any type of screen that partially shields radiation coming from the primary dipole-like

source placed inside the cavity [47]. For this reason, PRSs may take various forms that are conveniently categorized into three different classes [47] (see Figure 4):

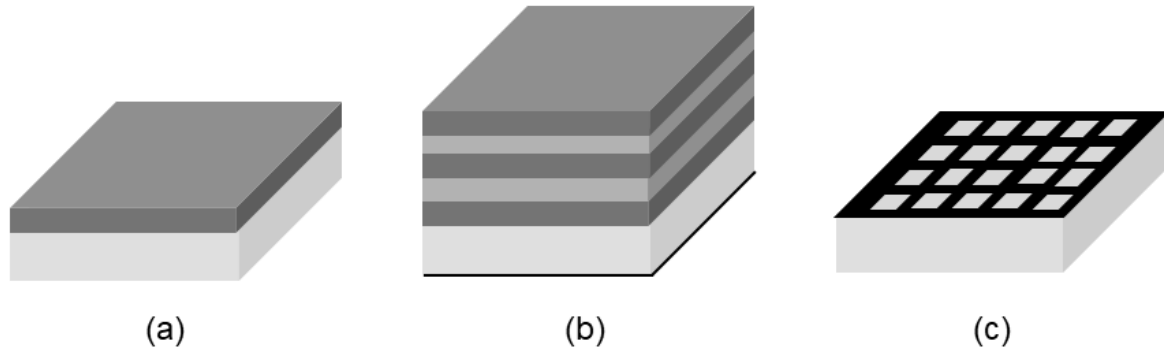


Figure 4. Schematic representation of Fabry–Perot cavity antennas with different physical implementation of their partially reflecting screen: (a) single-layer superstrate, (b) dielectric multilayer, and (c) homogenized metasurface. Different gray-scale colors represent different dielectric relative permittivities, while the black color represents metal areas.

- Single-layer dielectric covers which are typically implemented through a quarter-wavelength-thick high-permittivity slab [71,72];
- Dielectric multilayers consisting of alternating quarter-wavelength-thick slabs of high and low permittivity to realize a distributed Bragg reflector [73];
- Homogenized metasurfaces which are realized through subwavelength (with period $p \ll \lambda_0$) periodic planar arrangements of metal scatterers [74].

The last class is the most common at microwave frequencies and beyond to reduce dielectric losses [74]. This kind of PRS is rigorously represented by a tensor-like, frequency and spatially dispersive model given by an equivalent impedance of the kind $\underline{Z}_s(f, k_x, k_y)$. However, since FPCAs typically employ PRSs characterized by simple geometries and they are required to operate over a narrow FBW and/or at a fixed beam angle (or over a small angular variation) [74], the PRS is usually modeled as a single scalar, generally complex, sheet impedance $Z_s = R_s + jX_s$, with R_s and X_s being the equivalent resistance and reactance of the PRS, respectively. For lossless isotropic metasurfaces, this contribution is given by a scalar, purely imaginary, sheet impedance $Z_s = jX_s$. This assumption is valid for a large class of metasurfaces, even in the terahertz frequency range [74]. Typical examples, shown in Figure 3a, are 2-D patch arrays, metal strip gratings, and fishnet-like metasurfaces [64,65,74]. A method for the evaluation of such equivalent impedance value is shown in the following Section 3.3.

Depending on the nature of the PRS (viz., if the metasurface is inductive- or capacitive-like) and on the considered polarization, a variety of modes (i.e., surface, leaky, or plasmonic) can be generated. The generation of the different kinds of waves and their nature is deeply discussed in [75]. In this manuscript, we are just interested in leaky-wave modes for achieving an effective, compact, and directive radiating device. The application of the transverse resonance techniques [69] to the TEN implies equating to zero the sum of the input impedance or admittance looking downward and that looking upward at an arbitrary cross section of the equivalent transmission line. In this case study, it is convenient to assume $z = 0$ as a reference plane where the PRS is present (see Figure 3). In this manner, on the one side (the upper), there is the free-space characteristic admittance Y_0 , and, on the other side (the lower), there is the parallel admittance of the equivalent PRS admittance $Y_s = 1/Z_s$ (which is purely imaginary if the PRS is lossless, obtaining $Y_s = jB_s$, with $B_s = -1/X_s$) and of the short-circuited transmission-line section $Y_{sc} = -jY_d \cot \theta_0$. Therefore, the *dispersion equation* of the FPCA in presence of a lossless PRS reads:

$$Y_0 + Y_{sc} = Y_0 + jB_s - jY_d \cot(k_{zd}h) = 0 \quad (9)$$

It is worthwhile to point out that, in FPCAs able to produce a broadside pencil beam, by exciting the structure through an HED or an HMD both TE and TM modes are excited. It is thus important to report here the different quantities that appears in (9) for both polarizations, indicating with the hat $\hat{\cdot}$ the normalization with respect to the free-space wavenumber k_0 and with $\eta_0 = 120\pi \Omega$ the vacuum characteristic impedance.

$$Y_0^{\text{TE}} = \frac{\hat{k}_{z0}}{\eta_0}, \quad Y_d^{\text{TE}} = \frac{\hat{k}_{zd}}{\eta_0 \mu_r}, \quad \hat{k}_{zd} = \sqrt{\epsilon_r \mu_r - \hat{k}_\rho^2} \quad (10)$$

$$Y_0^{\text{TM}} = \frac{1}{\hat{k}_{z0} \eta_0}, \quad Y_d^{\text{TM}} = \frac{\epsilon_r}{\eta_0 \hat{k}_{zd}}, \quad \hat{k}_{zd} = \sqrt{\epsilon_r \mu_r - \hat{k}_\rho^2} \quad (11)$$

By considering a nonmagnetic material ($\mu_r = 1$) and by substituting Equations (10) or (11) in (9), the dispersion equation for TE:

$$\sqrt{1 - \hat{k}_\rho^2} + jB_s \eta_0 - j\sqrt{\epsilon_r - \hat{k}_\rho^2} \cot\left(k_0 h \sqrt{\epsilon_r - \hat{k}_\rho^2}\right) = 0 \quad (12)$$

or TM:

$$\left(\sqrt{1 - \hat{k}_\rho^2}\right)^{-1} + jB_s \eta_0 - j\left(\sqrt{\epsilon_r - \hat{k}_\rho^2}\right)^{-1} \cot\left[k_0 h \left(\sqrt{\epsilon_r - \hat{k}_\rho^2}\right)^{-1}\right] = 0 \quad (13)$$

modes are achieved, respectively. The zeros of Equations (12) and (13) can be found numerically through the *Padé* algorithm as clearly shown in [76]. In particular, by searching for the complex *improper* roots (i.e., with $\text{Im}[k_z] > 0$), the dispersion curves of the *leaky-wave modes* can be found and one can predict the radiating performance of the FPCAs under analysis.

3.3. Evaluation of the Equivalent Surface Impedance of a Partially Reflecting Sheet

The evaluation of the equivalent sheet impedance Z_s for a homogenized metasurface is a crucial step in the design of the realistic devices for FPCAs. A scalar sheet impedance Z_s , which generally depends on the polarization, can represent a planar patterned metal sheet if its periodicity p is much lower than the operative wavelength λ_0 . This assumption, which corresponds to the *homogenization principle*, is needed to let propagate only the fundamental $n = 0$ Floquet harmonic.

In order to evaluate the Z_s value, the unit cell of the homogenized metasurface is implemented on a commercial solver (such as CST Microwave Studio [77] or HFSS [78]) in a periodic environment (which means the application of *phase-shift* walls as boundary conditions on the periodicity directions). On top of the patterned metal, an air block is considered and, at the bottom, a grounded dielectric slab, where the metasurface lies, is assumed. In Figure 5, for instance, the case of a fishnet-like metasurface printed on top of a grounded dielectric slab of thickness h is considered.

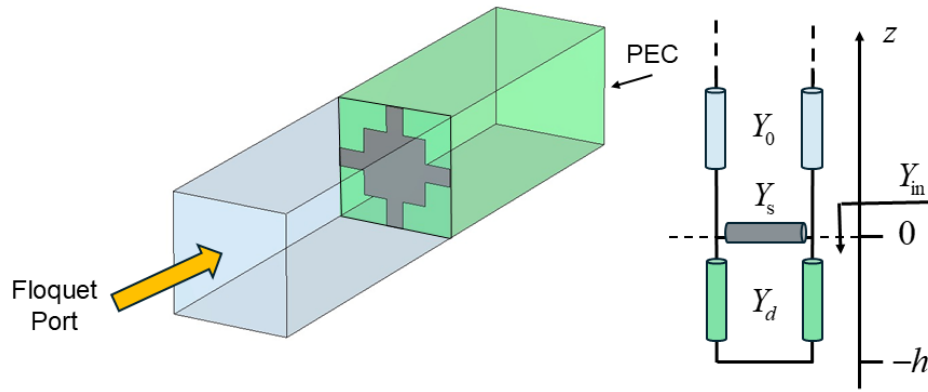


Figure 5. Full-wave model of a fishnet-like metasurface unit cell in a periodic environment on the left. A wave port is considered on top and it impinges on the homogenized-metasurface unit cell taking into account the substrate effect. On the bottom, a perfect-electric-conductor (PEC) condition is considered in order to represent the ground plane of the dielectric slab. On the right, the equivalent transmission-line model of the problem is shown.

By de-embedding the reference plane for the wave port shown in Figure 5 at the metasurface level ($z = 0$), the reflection coefficient S_{11} at the air-PRS interface is retrieved from the full-wave solver. At this point, one can easily evaluate the input admittance Y_{in} (see Figure 5) as:

$$Y_{in} = Y_0 \frac{1 - S_{11}}{1 + S_{11}} \quad (14)$$

where Y_0 is the vacuum characteristic admittance of the mode in propagation.

By observing the equivalent circuit in Figure 5, it is clear that Y_{in} , evaluated through a full-wave simulation, is given by the parallel of the homogenized-metasurface admittance Y_s and the input admittance of an h -thick, short-circuited, transmission-line segment with the dielectric characteristic admittance Y_d and propagation constant k_{zd} . Therefore, the desired Y_s value is straightforwardly evaluated as:

$$Y_s = Y_{in} - jY_d \cot(k_{zd}h) \quad (15)$$

Once the equivalent admittance is known, the evaluation of the equivalent sheet impedance of the homogenized metasurface is trivial:

$$Z_s = R_s + jX_s = 1/Y_s \quad (16)$$

with R_s equivalent resistance (which takes into account ohmic and dielectric losses) and X_s equivalent sheet reactance (in lossless material one commonly has $Z_s = jX_s$). The reactance sign can be either positive or negative representing an inductive- or capacitive-like metasurface, respectively.

In order to corroborate the proposed approach, an inductive-like partially reflecting sheet with X_s closed-form homogenization expressions is considered. In particular, a metal strip grating printed on air-like grounded dielectric slab with strip width w and periodicity p is assumed (see Figure 6). For this kind of unit cell, it has been demonstrated in [64] that:

$$X_s = -\frac{\eta_0 k_0 p}{2\pi} \ln \left(\csc \frac{\pi w}{2p} \right) \quad (17)$$

In Figure 6, for a fixed working frequency and periodicity, the equivalent reactance computed through full-wave simulations and theoretical formulas for different w/p filling factors are in a perfect agreement, thus corroborating the proposed approach.

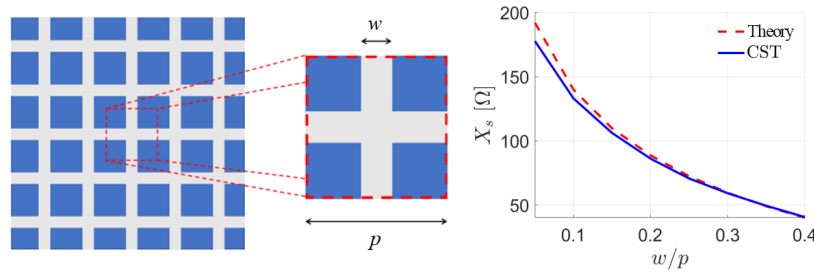


Figure 6. A schematic representation of a metal strip grating is reported on the left (metal and air are described in gray and blue, respectively). The equivalent reactance of the homogenized metasurface is reported on the right showing a remarkable agreement between the numerical analysis furnished in [64] and the proposed full-wave approach.

3.4. Feeding Schemes and Matching Networks

In this subsection, the physical implementation of the feeders of FPCAs is discussed. So far, ideal, dipole-like sources have been assumed. From a practical viewpoint, these kinds of feeders do not exist but they can be realized through devices having similar radiating features. Moreover, in order to avoid return-loss effects, which have been completely neglected so far, the feeding schemes have to be properly engineered to be perfectly matched. Such a goal is addressed in different manners depending on the considered source.

In the case of a VED-like feeder, a coaxial cable is commonly employed. The latter can be matched by efficiently choosing the penetration depth of its inner conductor and/or its dielectric filling in the FPCA. Moreover, a circular metallic patch can be properly designed in the center of the PRS as an additional element of the matching network. These parameters are usually optimized through parametric full-wave simulations [32,51,52,79]. A similar approach is commonly employed also for HED- and VMD-like sources, since they are implemented through bent coaxial cables in the FPCA, viz. an L probe [58] and a loop antenna [53,54], respectively. A particular attention is needed for HMDs. The latter are implemented through rectangular slots on the ground plane and, depending on their feeding scheme, they can be matched in different manners. For subresonant slots, a microstrip feeding network is commonly employed and it can be matched through standard transmission-line techniques [80,81]. In the case of quasi-resonant slots, the device can be fed through rectangular waveguides [33,57] whose return loss can be improved with different techniques [80]. In particular, an efficient transmission-line-based method that requires a single full-wave simulation to design capacitive irises has been proposed and validated in [55].

3.5. Full-Wave Validation of the Theoretical Model

This subsection simultaneously provides a rapid full-wave simulation setup for FPCAs and a validation of the theoretical leaky-wave model and of the correct antenna design. In order to do that, a case study is considered with an equivalent surface impedance $X_s = 30 \Omega$ and a dielectric slab with negligible losses (lossy cases are thoroughly discussed in [63]), thickness $h = 2.77$ mm, and relative permittivity $\epsilon_r = 3$. It is worthwhile to point out that the X_s , ϵ_r , and h values can be properly designed to achieve the desired radiating features at a certain frequency f_0 , as previously discussed in Section 3.1.

Once the design parameters of the proposed FPCA are fixed, one can easily evaluate the leaky-wave dispersion curves through the transverse resonance technique applied to the TEN of the device, as thoroughly discussed in Section 3.2. In this manner, the profile of the phase and attenuation constant normalized with respect to the vacuum wavenumber k_0 , viz. $\hat{\beta} = \beta/k_0$ and $\hat{\alpha} = \alpha/k_0$, respectively, are retrieved vs. frequency f , as shown in Figure 7a. From the dispersion curves, it is clear that the proposed device is able to generate a pencil beam with the maximum radiated power at broadside at $f_c = 29.88$ GHz, when $\beta^{\text{TE}} \simeq \alpha^{\text{TE}} \simeq \beta^{\text{TM}} \simeq \alpha^{\text{TM}}$ [66]. Moreover, as previously discussed in Section 3.2, one can assert that the device is working in the reactive regime for $f < f_c$ [67] and it is generating a

conical beam for $f > f_c$. By exploiting the evaluation of the dispersion curves, it is also possible to choose the lateral extension of the device in order to achieve a radiation efficiency of, at least, 90 % at a certain working frequency $f_w = 33$ GHz. In particular, by considering $\alpha = \min\{\alpha^{\text{TE}}(f_w), \alpha^{\text{TM}}(f_w)\}$, the minimum extension of the radiating device is set at $L = 38.96$ mm through (2).

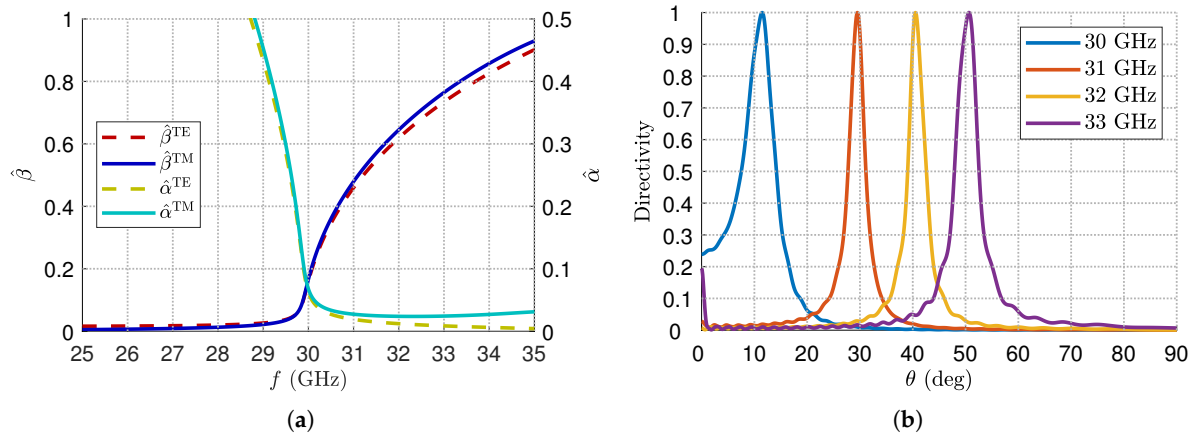


Figure 7. (a) Dispersion curves of both the TE and TM modes of the phase $\hat{\beta}$ and attenuation $\hat{\alpha}$ constants normalized with respect to the vacuum wavenumber k_0 . (b) Radiation patterns, normalized with respect to their maximum in a linear scale, of the simulated FPCA at different frequencies.

Once the minimum lateral dimension of the FPCA has been found, the device is ready to be simulated on a commercial full-wave solver to verify its radiation property. In order to do that and to strongly reduce the computational effort, one can implement the source as an ideal dipole (its physical implementation and matching techniques have been discussed in Section 3.4) and the PRS through a surface impedance boundary condition (SIBC) —the design of the real reflecting layer can be addressed through a homogenized metasurface designed with the approach shown in Section 3.3. It is worthwhile to point out that the SIBC has to be described with a frequency-dispersive behavior which respects the Foster's reactance theorem [82]. Therefore, depending on the inductive-like or capacitive-like nature of the PRS, one has to enforce on the full-wave solver $Z_s = j\omega L$ or $Z_s = -j/\omega C$, respectively. Specifically, the lumped inductance L and capacitance C value are fixed so as to match the desired X_s value at the working frequency of the design.

By applying the simulation guidelines discussed so far, a three-dimensional (3-D) model of the proposed FPCA has been implemented on CST Microwave Studio [77] through a transparent SIBC on top of a cylindrical grounded dielectric slab with height $h = 2.77$ mm, aperture diameter $L = 40$ mm, and relative permittivity $\epsilon_r = 3$. By exciting the device through an HED in the middle of the cavity [44], the far-field radiation patterns for $f > f_c$ reported in Figure 7(b) are achieved. The generation of conical beams, with a scanning pointing angle θ_0 which varies as the frequency increases through (4), is thus demonstrated.

4. Radially Periodic Leaky-Wave Antennas

This section deals with the analysis of radially periodic LWAs. Since the latter are constituted by a two-dimensional, leaky-wave, radiating devices, the design rules in terms of directivity and fractional bandwidth as a function of the leaky phase and attenuation constants are the same as those presented in Section 3.1. The main difference lies on the evaluation method of β and α . In FPCAs it is indeed possible to consider the PRS in the homogenization regime and, thus, to exploit the transverse resonance technique applied to the TEN of the device. In radially periodic LWAs, the periodicity of the annular metal strip grating printed on top of the GDS is instead comparable to the operating wavelength λ_0 and the radiation is usually related to the first-order, fast, Floquet-Bloch mode in propagation [31,79]. It is here provided a simple technique for the Bloch analysis in Section 4.1 and validated in Section 4.2 through full-wave simulation of the entire structure.

4.1. A Simple Technique for the Bloch Analysis

As abovementioned, a two-dimensional radially periodic LWA is constituted by a subwavelength-thick grounded dielectric slab with an annular metal strip on top (see Figure 2e) [48]. By considering an azimuthal symmetric source, such as a VED, it is possible to consider a local linearization of the radial structure as a 1-D periodic metal-strip grating, which can be described in terms of space harmonics [48]. The radial leaky-wave propagation over an annular metal-strip grating can indeed be seen as a 1-D propagation over an infinite metal strip grating with phase advance normal to the printed strips thanks to the azimuthal symmetry of the device [48]. This aspect is well explained in Figure 8 where the linearization process for an azimuthally symmetric radial periodicity on a 2-D structure is straightforwardly reported.

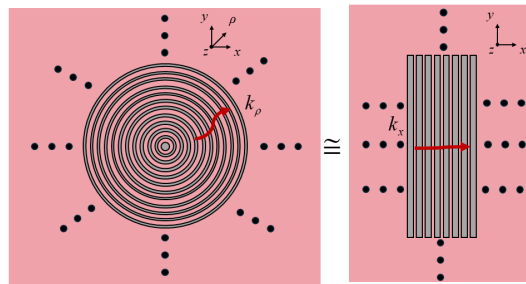


Figure 8. The complex leaky radial wavenumber, k_{ρ} , of the radially periodic LWA (represented on the left) can be approximately seen as the leaky-wave propagation constant of an infinite metal strip grating with phase advance normal to the printed strips (as shown on the right) [48].

The device can thus be analyzed as a 1-D periodic LWA. In this context, the generic m -th Floquet space harmonic (with $m = 0, \pm 1, \pm 2, \dots$) has a dispersive behavior related to the fundamental harmonic wavenumber $k_{\rho 0} = \beta_0 - j\alpha$ and the periodicity (along the radial direction) p as follows:

$$k_{\rho m} = \beta_0 + \frac{2\pi m}{p} - j\alpha \quad (18)$$

The structure is usually designed to let the $m = -1$ harmonic propagate in the working frequency range. Therefore, it is manifest that, also in this case, the correct evaluation of the leaky wavenumber plays a fundamental role in the theoretical design and performance evaluation of the LWA. In this context, the possibility to describe the device through its linearized counterpart [48] (see Figure 8) is crucial for the evaluation of the leaky radial wavenumber. This is because different techniques have been already proposed for retrieving the dispersion diagram of leaky modes propagating in 1-D periodic LWAs (see, e.g., [83–86] and reference therein).

In this paper, in order to avoid the implementation of an ad-hoc method-of-moments (MoM) approach for the considered structures [83], the need for complicated numerical routines [85], or the correct selection of higher-order modes in the simulation model [84], a method originally proposed for the analysis of *frozen* modes is exploited [87].

In order to corroborate the proposed approach, the reference case in [79] is considered since the dispersion curves are there retrieved through a MoM [83]. While, in [79], the radially periodic device was considered as a wideband Bessel-beam launcher (BBL) in the near-field region, the same structure will be considered here as a LWA in the far-field region. The wideband BBL proposed in [79] works with a central frequency $f_0 = 23$ GHz through a GDS with relative permittivity $\epsilon_r = 2.2$ and thickness $h = 3.14$ mm perturbed by a metal strip grating with periodicity $p = 10$ mm and slot width $s = 6$ mm (see Figure 9a).

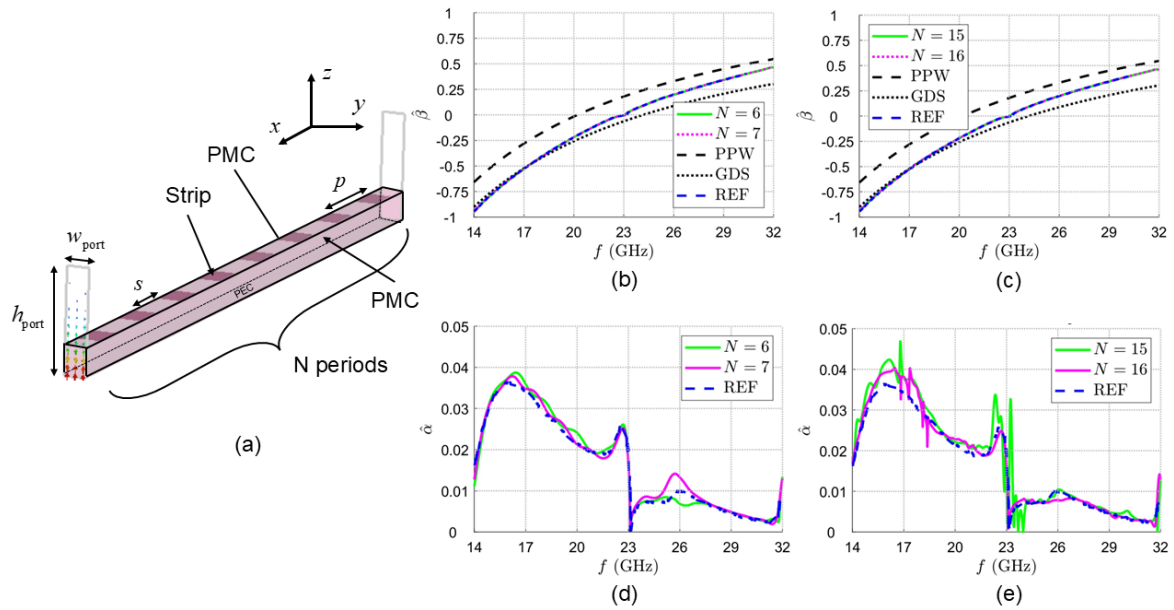


Figure 9. (a) Schematic representation of the full-wave model of the linearized counterpart of the radially periodic 2-D LWA constituted by a grounded dielectric slab (pink solid) with N unit cells of a metal strip grating on top (gray areas). The two rectangular areas delimited by light-gray lines represent the two considered waveguide ports. In one of them, the modal field distribution is reported through lines of force, showing the correct excitation of the TM_0 mode in the device. (b)–(e) Dispersion diagrams of the normalized leaky ((b) and (c)) phase $\hat{\beta}$ and ((d) and (e)) attenuation $\hat{\alpha}$ constants. While the blue dashed lines represent the reference case obtained through a MoM approach [79], black dashed and dotted lines represent the limiting, unperturbed cases of a parallel-plate waveguide (PPW) and of a grounded dielectric slab (GDS) structure, respectively. The green and magenta colors represent two subsequent case studies: $N = 6$ and $N = 7$ for (b) and (d), $N = 15$ and $N = 16$ for (c) and (e).

In order to apply the approach proposed in [87], two waveguide ports are here defined in the periodic direction with a height $h_{\text{port}} = 3.5h$ and lateral dimension $w_{\text{port}} = \lambda_0/4$ such that the fundamental TM_0 surface wave of the grounded dielectric slab is properly represented. Perfect-magnetic-conductor (PMC) boundaries and an open boundary condition are assigned along y and z (see Figure 9a), respectively.

At this point, the transfer matrix of the single unit cell is extracted with CST full-wave simulations [77] by multiplying the transfer matrix obtained simulating $N + 1$ unit cells with the inverse of the one with N unit cells [87]. The T matrix of the single unit cell, which takes into account the mutual coupling of adjacent cells, can thus be found. Then, the leaky phase and attenuation constants can be derived through well-known formulas [80,84,86]. As shown in Figure 9b (for the two case studies $N = 6$ and $N = 7$) and (c) (for the two case studies $N = 15$ and $N = 16$), this method perfectly evaluates the phase constant β regardless the number of periods utilized in the analysis. This is not the case for the evaluation of the leakage constants as shown in Figure 9d,e, since the evaluation of α is typically more difficult [86]. By adding unit cells in the CST simulation, indeed, the only effect is to introduce additional numerical noise. This is due to the fact that α represents an amplitude decay and, by considering high values of N , the evaluation of this parameter is performed over distances at which most of the power has been already radiated by the equivalent 1-D periodic LWA implemented on CST. On the other hand, a small number of periods does not represent well the mutual coupling among unit cells.

By observing the dispersion curves of the leaky phase and attenuation constants, it is clear the presence of the open-stopband phenomenon which is related to the controdirectional coupling between two Floquet-Bloch harmonics [29]. When β tends to zero, indeed, the value of α changes rapidly avoiding the proper generation of a beam at broadside [29]: first, it exhibits a highly peaked behavior due to an accumulation of reactive energy, and then drops to zero at the broadside frequency [3]. Although this aspect goes beyond the interest of this paper, it is worthwhile to point out that

different techniques were proposed to mitigate or suppress the open stopband, thereby improving the near-field [88] or far-field radiating properties of 1-D or 2-D LWAs [89,90].

4.2. Full-Wave Validation of the Theoretical Model

In this subsection, the 3-D model of the radially periodic LWA studied in [79] has been simulated in CST Microwave Studio with the aim of deriving its far-field radiation pattern. Results are reported in Figure 10 through 3-D radiation patterns normalized with respect to their maximum in a linear scale. As expected, the device generates a conical beam in the far-field region with the pointing angle θ_0 which decreases as the frequency increases from 17 GHz to 20 GHz. This aspect is in perfect agreement with the dispersion curves reported in Figure 9 since the absolute value of β decreases in that frequency range and, thus, θ_0 decreases, as expected from (4).

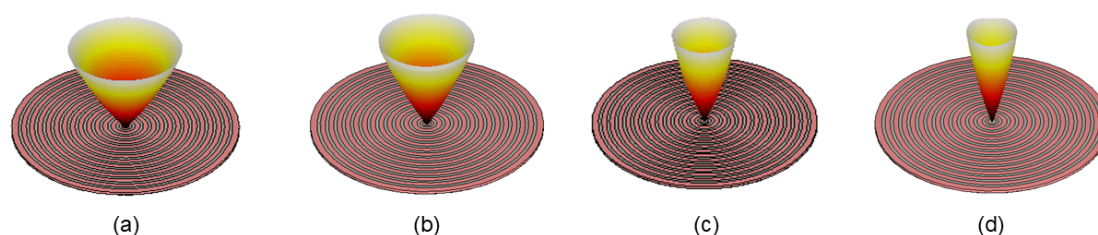


Figure 10. Three-dimensional radiation pattern of the considered radially periodic LWA in a linear scale at (a) 17 GHz, (b) 18 GHz, (c) 19 GHz, and (d) 20 GHz.

5. Conclusions

This paper provides a simple guideline for the characterization and design of uniform, quasi-uniform, and radially periodic two-dimensional leaky-wave antennas from theoretical, numerical, and simulative viewpoints.

In particular, as concerns the analysis of Fabry–Perot leaky-wave antennas, different techniques and methods are reviewed: the leaky-wave approach for predicting and designing the performance of the radiating device, the application of the transverse resonance technique to the transverse equivalent network of the antenna, the evaluation and design of a desired equivalent sheet impedance through homogenized metasurfaces, and the correct choice and implementation of a realistic feeder. As concerns radially periodic leaky-wave antennas, a simple technique for the Bloch analysis is proposed and corroborated. Moreover, all the proposed designs are verified through full-wave simulations, confirming the validity of the proposed approaches for a simple, effective, and fast design of different kinds of leaky-wave antennas.

Author Contributions: Conceptualization, E.N. and W.F.; methodology, E.N. and W.F.; software, E.N. and W.F.; validation, E.N.; formal analysis, E.N., W.F., P.B., and A.G.; investigation, E.N.; resources, E.N. and W.F.; data curation, E.N.; writing—original draft preparation, E.N.; writing—review and editing, E.N., W.F., P.B., and A.G.; visualization, E.N.; supervision, W.F., P.B., and A.G.; project administration, W.F., P.B., and A.G.; funding acquisition, W.F. and A.G. All authors have read and agreed to the published version of the manuscript.

Funding: This work was supported by the European Union - Next Generation EU under the Italian National Recovery and Resilience Plan (NRRP), Mission 4, Component 2, Investment 1.3, CUP B53C22004050001, partnership on “Telecommunications of the Future” (PE00000001 - program “RESTART”).

Institutional Review Board Statement: Not applicable

Informed Consent Statement: Not applicable

Data Availability Statement: The original contributions presented in this study are included in the article. Further inquiries can be directed to the corresponding author.

Conflicts of Interest: The authors declare no conflicts of interest

Abbreviations

The following abbreviations are used in this manuscript:

| | |
|------|-------------------------------|
| 1-D | One Dimension |
| 2-D | Two Dimension |
| 3-D | Three Dimension |
| BBL | Bessel-Beam Launcher |
| FBW | Fractional Bandwidth |
| FoM | Figure of Merit |
| FPCA | Fabry–Perot Cavity Antenna |
| GDS | Grounded Dielectric Slab |
| HED | Horizontal Electric Dipole |
| HMD | Horizontal Magnetic Dipole |
| HPBW | Half-Power Beamwidth |
| LWA | Leaky-Wave Antenna |
| MoM | Method of Moments |
| PEC | Perfect Electric Conductor |
| PMC | Perfect Magnetic Conductor |
| PPW | Parallel-Plate Waveguide |
| PRS | Partially Reflecting Sheet |
| TEN | Transverse Equivalent Network |
| VED | Vertical Electric Dipole |
| VMD | Vertical Magnetic Dipole |

References

1. Jackson, D.R.; Caloz, C.; Itoh, T. Leaky-wave antennas. *Proc. IEEE* **2012**, *100*, 2194–2206.
2. Monticone, F.; Alù, A. Leaky-Wave Theory, Techniques, and Applications: From Microwaves to Visible Frequencies. *Proc. IEEE* **2015**, *103*, 793–821. <https://doi.org/10.1109/JPROC.2015.2399419>.
3. Oliner, A.A.; Jackson, D.R.; Volakis, J. Leaky-wave antennas. *Antenna engineering handbook* **2007**, *4*, 12.
4. Marcuvitz, N. On field representations in terms of leaky modes or eigenmodes. *IRE Trans. Antennas Propag.* **1956**, *4*, 192–194.
5. Tamir, T.; Oliner, A.A. Guided complex waves. Part 1: Fields at an interface. *Proc. IEE* **1963**, *110*, 310–324.
6. Tamir, T.; Oliner, A.A. Guided complex waves. Part 2: Relation to radiation patterns. *Proc. IEE* **1963**, *110*, 325–334.
7. Balanis, C.A. *Antenna Theory: Analysis and Design*; Wiley, 2015.
8. Galli, A.; Baccarelli, P.; Burghignoli, P. Leaky-Wave Antennas. *Wiley Encyclopedia of Electrical and Electronics Engineering* **2016**, pp. 1–20.
9. Wang, M.; Ma, H.F.; Zhang, H.C.; Tang, W.X.; Zhang, X.R.; Cui, T.J. Frequency-Fixed Beam-Scanning Leaky-Wave Antenna Using Electronically Controllable Corrugated Microstrip Line. *IEEE Trans. Antennas Propag.* **2018**, *66*, 4449–4457. <https://doi.org/10.1109/TAP.2018.2845452>.
10. Kodera, T.; Caloz, C. Uniform Ferrite-Loaded Open Waveguide Structure With CRLH Response and Its Application to a Novel Backfire-to-Endfire Leaky-Wave Antenna. *IEEE Trans. Microw. Theory Techn.* **2009**, *57*, 784–795. <https://doi.org/10.1109/TMTT.2009.2015070>.
11. Chang, L.; Zhang, Z.; Li, Y.; Wang, S.; Feng, Z. 60-GHz Air Substrate Leaky-Wave Antenna Based on MEMS Micromachining Technology. *IEEE Trans. Compon. Packag. Manuf. Technol.* **2016**, *6*, 1656–1662. <https://doi.org/10.1109/TCPMT.2016.2616516>.
12. Buzzin, A.; Asquini, R.; Caputo, D.; de Cesare, G. Sensitive and Compact Evanescent-Waveguide Optical Detector for Sugar Sensing in Commercial Beverages. *Sensors* **2023**, *23*. <https://doi.org/10.3390/s23198184>.
13. Fuscaldo, W.; Burghignoli, P.; Baccarelli, P.; Galli, A. Graphene Fabry–Perot Cavity Leaky-Wave Antennas: Plasmonic Versus Nonplasmonic Solutions. *IEEE Trans. Antennas Propag.* **2017**, *65*, 1651–1660. <https://doi.org/10.1109/TAP.2017.2670520>.
14. Wang, X.C.; Zhao, W.S.; Hu, J.; Yin, W.Y. Reconfigurable terahertz leaky-wave antenna using graphene-based high-impedance surface. *IEEE Trans. Nanotechnol.* **2015**, *14*, 62–69.

15. Jiang, D.; Li, X.; Fu, Z.; Ran, P.; Wang, G.; Zheng, Z.; Zhang, T.; Wang, W.Q. Liquid Crystal-Based Wideband Reconfigurable Leaky Wave X-Band Antenna. *IEEE Access* **2019**, *7*, 127320–127326. <https://doi.org/10.1109/ACCESS.2019.2939097>.
16. Almutawa, A.T.; Hosseini, A.; Jackson, D.R.; Capolino, F. Leaky-wave analysis of wideband planar Fabry–Pérot cavity antennas formed by a thick PRS. *IEEE Trans. Antennas Propag.* **2019**, *67*, 5163–5175.
17. Al-Tarifi, M.A.; Anagnostou, D.E.; Amert, A.K.; Whites, K.W. Bandwidth enhancement of the resonant cavity antenna by using two dielectric superstrates. *IEEE Trans. Antennas Propag.* **2013**, *61*, 1898–1908.
18. Baba, A.A.; Hashmi, R.M.; Esselle, K.P. Achieving a Large Gain-Bandwidth Product From a Compact Antenna. *IEEE Trans. Antennas Propag.* **2017**, *65*, 3437–3446. <https://doi.org/10.1109/TAP.2017.2700016>.
19. Baba, A.A.; Hashmi, R.M.; Esselle, K.P.; Weily, A.R. Compact High-Gain Antenna With Simple All-Dielectric Partially Reflecting Surface. *IEEE Trans. Antennas Propag.* **2018**, *66*, 4343–4348. <https://doi.org/10.1109/TAP.2018.2842247>.
20. Karmokar, D.K.; Esselle, K.P.; Hay, S.G. Fixed-Frequency Beam Steering of Microstrip Leaky-Wave Antennas Using Binary Switches. *IEEE Trans. Antennas Propag.* **2016**, *64*, 2146–2154. <https://doi.org/10.1109/TAP.2016.2546949>.
21. Javanbakht, N.; Syrett, B.; Amaya, R.E.; Shaker, J. A Review of Reconfigurable Leaky-Wave Antennas. *IEEE Access* **2021**, *9*, 94224–94238. <https://doi.org/10.1109/ACCESS.2021.3093775>.
22. Negri, E.; Fuscaldo, W.; Burghignoli, P.; Galli, A. Reconfigurable THz leaky-wave antennas based on innovative metal–graphene metasurfaces. *J. Phys. D: Appl. Phys.* **2024**.
23. Gomez-Tornero, J.; Martinez, A.; Rebenaque, D.; Gugliemi, M.; Alvarez-Melcon, A. Design of tapered leaky-wave antennas in hybrid waveguide-planar technology for millimeter waveband applications. *IEEE Trans. Antennas Propag.* **2005**, *53*, 2563–2577. <https://doi.org/10.1109/TAP.2005.850741>.
24. Gomez-Tornero, J.L. Analysis and Design of Conformal Tapered Leaky-Wave Antennas. *IEEE Antennas Wirel. Propag. Letters* **2011**, *10*, 1068–1071. <https://doi.org/10.1109/LAWP.2011.2170051>.
25. Fong, B.; Colburn, J.S.; Ottusch, J.J.; Visher, J.; Sevenpiper, D. Scalar and tensor holographic artificial impedance surfaces. *IEEE Trans. Antennas Propag.* **2010**, *58*, 3212–3221.
26. Minatti, G.; Caminita, F.; Casaletti, M.; Maci, S. Spiral leaky-wave antennas based on modulated surface impedance. *IEEE Trans. Antennas Propag.* **2011**, *59*, 4436–4444.
27. Minatti, G.; Faenzi, M.; Martini, E.; Caminita, F.; De Vita, P.; González-Ovejero, D.; Sabbadini, M.; Maci, S. Modulated metasurface antennas for space: Synthesis, analysis and realizations. *IEEE Trans. Antennas Propag.* **2014**, *63*, 1288–1300.
28. Faenzi, M.; Caminita, F.; Martini, E.; De Vita, P.; Minatti, G.; Sabbadini, M.; Maci, S. Realization and measurement of broadside beam modulated metasurface antennas. *IEEE Antennas Wirel. Propag. Letters* **2015**, *15*, 610–613.
29. Giusti, F.; Maci, S.; Martini, E. Complete Open-Stopband Suppression Using Sinusoidally Modulated Anisotropic Metasurfaces. *IEEE Trans. Antennas Propag.* **2023**, *71*, 8537–8547.
30. Ettorre, M.; Pavone, S.C.; Casaletti, M.; Albani, M.; Mazzinghi, A.; Freni, A. Near-field focusing by non-diffracting Bessel beams. In *Aperture Antennas for Millimeter and Sub-Millimeter Wave Applications*; Springer: Cham, Switzerland, 2018; pp. 243–288.
31. Negri, E.; Fuscaldo, W.; González-Ovejero, D.; Burghignoli, P.; Galli, A. TE-Polarized Leaky-Wave Beam Launchers: Generation of Bessel and Bessel–Gauss Beams. *Appl. Phys. Letters* **2024**, *125*, 181703.
32. Fuscaldo, W.; Valerio, G.; Galli, A.; Sauleau, R.; Grbic, A.; Ettorre, M. Higher-order leaky-mode Bessel-beam launcher. *IEEE Trans. Antennas Propag.* **2016**, *64*, 904–913.
33. Negri, E.; Fuscaldo, W.; Burghignoli, P.; Galli, A. Leaky-Wave Analysis of TM-, TE-, and Hybrid-Polarized Aperture-Fed Bessel-Beam Launchers for Wireless Power Transfer Links. *IEEE Trans. Antennas Propag.* **2023**, *71*, 1424–1436. <https://doi.org/10.1109/TAP.2022.3231086>.
34. Hansen, W.W. Radiating electromagnetic wave guide. *US Patent 2,402,622* **1946**.
35. Goldstone, L.; Oliner, A.A. Leaky-wave antennas I: Rectangular waveguides. *IRE Trans. Antennas Propag.* **1959**, *7*, 307–319. <https://doi.org/10.1109/TAP.1959.1144702>.
36. Goldstone, L.; Oliner, A.A. Leaky wave antennas II: Circular waveguides. *IRE Trans. Antennas Propag.* **1961**, *9*, 280–290. <https://doi.org/10.1109/TAP.1961.1144995>.
37. Hines, J.N.; Rumsey, V.H.; Walter, C.H. Traveling-wave slot antennas. *Proc. IRE* **1953**, *41*, 1624–1631.
38. Collin, R.E.; Zucker, F.J. *Antenna Theory*; Number pt. 7, No. 1, McGraw-Hill, 1969.
39. Rezaee, S.; Memarian, M. Analytical Study of Open-Stopband Suppression in Leaky-Wave Antennas. *IEEE Antennas Wirel. Propag. Letters* **2020**, *19*, 363–367. <https://doi.org/10.1109/LAWP.2019.2963798>.

40. Otto, S.; Al-Bassam, A.; Rennings, A.; Solbach, K.; Caloz, C. Transversal Asymmetry in Periodic Leaky-Wave Antennas for Bloch Impedance and Radiation Efficiency Equalization Through Broadside. *IEEE Trans. Antennas Propag.* **2014**, *62*, 5037–5054. <https://doi.org/10.1109/TAP.2014.2343621>.
41. Otto, S.; Al-Bassam, A.; Rennings, A.; Solbach, K.; Caloz, C. Radiation Efficiency of Longitudinally Symmetric and Asymmetric Periodic Leaky-Wave Antennas. *IEEE Antennas Wirel. Propag. Letters* **2012**, *11*, 612–615. <https://doi.org/10.1109/LAWP.2012.2202365>.
42. Ip, A.; Jackson, D.R. Radiation from cylindrical leaky waves. *IEEE Trans. Antennas Propag.* **1990**, *38*, 482–488. <https://doi.org/10.1109/8.52266>.
43. Madji, M.; Negri, E.; Fuscaldo, W.; Comite, D.; Galli, A.; Burghignoli, P. The Leaky-Wave Perspective for Array-Fed Fabry-Perot Cavity and Bull's-Eye Antennas. *Appl. Sci.* **2024**, *14*. <https://doi.org/10.3390/app14156775>.
44. Madji, M.; Negri, E.; Fuscaldo, W.; Comite, D.; Galli, A.; Burghignoli, P. Two-Dimensional Scanning of Circularly Polarized Beams via Array-Fed Fabry-Perot Cavity Antennas. *Appl. Sci.* **2024**, *14*. <https://doi.org/10.3390/app142412058>.
45. Xie, P.; Wang, G.; Li, H.; Liang, J.; Gao, X. Circularly Polarized Fabry-Perot Antenna Employing a Receiver-Transmitter Polarization Conversion Metasurface. *IEEE Trans. Antennas Propag.* **2019**, *68*, 3213–3218. <https://doi.org/10.1109/TAP.2019.2950811>.
46. Huang, Y.; Yang, L.; Li, J.; Wang, Y.; Wen, G. Polarization conversion of metasurface for the application of wide band low-profile circular polarization slot antenna. *Appl. Phys. Lett.* **2016**, *109*.
47. Burghignoli, P.; Fuscaldo, W.; Galli, A. Fabry-Perot Cavity Antennas: The Leaky-Wave Perspective. *IEEE Antennas Propag. Mag.* **2021**, *63*, 116–145.
48. Podilchak, S.K.; Baccarelli, P.; Burghignoli, P.; Freundorfer, A.P.; Antar, Y.M.M. Analysis and Design of Annular Microstrip-Based Planar Periodic Leaky-Wave Antennas. *IEEE Trans. Antennas Propag.* **2014**, *62*, 2978–2991. <https://doi.org/10.1109/TAP.2014.2314735>.
49. Sengupta, S.; Jackson, D.R.; Long, S.A. Modal Analysis and Propagation Characteristics of Leaky Waves on a 2-D Periodic Leaky-Wave Antenna. *IEEE Trans. Microw. Theory Techn.* **2018**, *66*, 1181–1191. <https://doi.org/10.1109/TMTT.2017.2783373>.
50. Fuscaldo, W.; Galli, A.; Jackson, D.R. Optimization of 1-D Unidirectional Leaky-Wave Antennas Based on Partially Reflecting Sheets. *IEEE Trans. Antennas Propag.* **2022**, *70*, 7853–7868.
51. Ettorre, M.; Grbic, A. Generation of propagating Bessel beams using leaky-wave modes. *IEEE Trans. Antennas Propag.* **2012**, *60*, 3605–3613. <https://doi.org/10.1109/TAP.2012.2201088>.
52. Ettorre, M.; Rudolph, S.M.; Grbic, A. Generation of propagating Bessel beams using leaky-wave modes: experimental validation. *IEEE Trans. Antennas Propag.* **2012**, *60*, 2645–2653.
53. Lu, P.; Bréard, A.; Huillery, J.; Yang, X.S.; Voyer, D. Feeding coils design for TE-polarized Bessel antenna to generate rotationally symmetric magnetic field distribution. *IEEE Antennas Wireless Propag. Lett.* **2018**, *17*, 2424–2428. <https://doi.org/10.1109/LAWP.2018.2877038>.
54. Lu, P.; Voyer, D.; Bréard, A.; Huillery, J.; Allard, B.; Lin-Shi, X.; Yang, X.S. Design of TE-polarized Bessel antenna in microwave range using leaky-wave modes. *IEEE Trans. Antennas Propag.* **2017**, *66*, 32–41.
55. Negri, E.; Fuscaldo, W.; Tofani, S.; Burghignoli, P.; Galli, A. An efficient and accurate semi-analytical matching technique for waveguide-fed antennas. *Sci. Rep.* **2024**, *14*, 3892.
56. Feresidis, A.; Vardaxoglou, J. High gain planar antenna using optimised partially reflective surfaces. *IEE Proc. Microwaves, Antennas Propag* **2001**, *148*, 345–350(5).
57. Scattone, F.; Ettorre, M.; Sauleau, R.; Nguyen, N.T.; Fonseca, N.J. Optimization procedure for planar leaky-wave antennas with flat-topped radiation patterns. *IEEE Trans. Antennas Propag.* **2015**, *63*, 5854–5859.
58. Guo, Y.X.; Chia, M.; Chen, Z.N.; Luk, K.M. Wide-band L-probe fed circular patch antenna for conical-pattern radiation. *IEEE Trans. Antennas Propag.* **2004**, *52*, 1115–1116. <https://doi.org/10.1109/TAP.2004.823971>.
59. Mateo-Segura, C.; Feresidis, A.P.; Goussetis, G. Bandwidth Enhancement of 2-D Leaky-Wave Antennas With Double-Layer Periodic Surfaces. *IEEE Trans. Antennas Propag.* **2013**, *62*, 586–593. <https://doi.org/10.1109/TAP.2013.2292076>.
60. Von Trentini, G. Partially reflecting sheet arrays. *IRE Trans. Antennas Propag.* **1956**, *4*, 666–671.
61. Jackson, D.R.; Burghignoli, P.; Lovat, G.; Capolino, F.; Chen, J.; Wilton, D.R.; Oliner, A.A. The Fundamental Physics of Directive Beaming at Microwave and Optical Frequencies and the Role of Leaky Waves. *Proc. IEEE* **2011**, *99*, 1780–1805. <https://doi.org/10.1109/JPROC.2010.2103530>.
62. Zhao, T.; Jackson, D.; Williams, J.; Oliner, A. General formulas for 2-D leaky-wave antennas. *IEEE Trans. Antennas Propag.* **2005**, *53*, 3525–3533. <https://doi.org/10.1109/TAP.2005.856315>.

63. Fuscaldo, W. Rigorous evaluation of losses in uniform leaky-wave antennas. *IEEE Trans. Antennas Propag.* **2020**, *68*, 643–655.
64. Luukkonen, O.; Simovski, C.; Granet, G.; Goussetis, G.; Lioubtchenko, D.; Raisanen, A.V.; Tretyakov, S.A. Simple and accurate analytical model of planar grids and high-impedance surfaces comprising metal strips or patches. *IEEE Trans. Antennas Propag.* **2008**, *56*, 1624–1632.
65. Tretyakov, S. *Analytical Modeling in Applied Electromagnetics*; Artech House: Norwood, MA, USA, 2003.
66. Lovat, G.; Burghignoli, P.; Jackson, D.R. Fundamental properties and optimization of broadside radiation from uniform leaky-wave antennas. *IEEE Trans. Antennas Propag.* **2006**, *54*, 1442–1452. <https://doi.org/10.1109/TAP.2006.874350>.
67. Fuscaldo, W.; Burghignoli, P.; Galli, A. The transition between reactive and radiative regimes for leaky modes in planar waveguides based on homogenized partially reflecting surfaces. *IEEE Trans. Microw. Theory Techn.* **2020**, *68*, 5259–5269.
68. Balanis, C.A. *Advanced Engineering Electromagnetics*; Wiley & Sons: New York, NY: Wiley, 2012.
69. Sorrentino, R.; Mongiardo, M. *Transverse Resonance Techniques*; John Wiley & Sons, Ltd: New York, NY, USA, 2005. <https://doi.org/10.1002/0471654507.eme465>.
70. Felsen, L.B.; Marcuvitz, N. *Radiation and Scattering of Waves*; Vol. 31, John Wiley & Sons, 1994.
71. Jackson, D.R.; Oliner, A.A. A leaky-wave analysis of the high-gain printed antenna configuration. *IEEE Trans. Antennas Propag.* **1988**, *36*, 905–910. <https://doi.org/10.1109/8.7194>.
72. Jackson, D.R.; Alexopoulos, N.G. Gain enhancement methods for printed circuit antennas. *IEEE Trans. Antennas Propag.* **1985**, *33*, 976–987. <https://doi.org/10.1109/TAP.1985.1143709>.
73. Jackson, D.R.; Oliner, A.A.; Ip, A. Leaky-wave propagation and radiation for a narrow-beam multiple-layer dielectric structure. *IEEE Trans. Antennas Propag.* **1993**, *41*, 344–348. <https://doi.org/10.1109/8.233128>.
74. Fuscaldo, W.; Tofani, S.; Zografopoulos, D.C.; Baccarelli, P.; Burghignoli, P.; Beccherelli, R.; Galli, A. Systematic design of THz leaky-wave antennas based on homogenized metasurfaces. *IEEE Trans. Antennas Propag.* **2018**, *66*, 1169–1178.
75. Fuscaldo, W.; Burghignoli, P.; Galli, A. Genealogy of Leaky, Surface, and Plasmonic Modes in Partially Open Waveguides. *Phys. Rev. Appl.* **2022**, *17*, 034–038.
76. Galdi, V.; Pinto, I.M. A simple algorithm for accurate location of leaky-wave poles for grounded inhomogeneous dielectric slabs. *Microw. Opt. Techn. Lett.* **2000**, *24*, 135–140.
77. CST products Dassault Systèmes, France, 2021.
78. Ansys Corporation, Ansys HFSS Version 16.0, 1984-2016.
79. Comite, D.; Fuscaldo, W.; Podilchak, S.K.; Hilarío-Re, P.D.; Gómez-Guillamón Buendía, V.; Burghignoli, P.; Baccarelli, P.; Galli, A. Radially Periodic Leaky-Wave Antenna for Bessel Beam Generation Over a Wide-Frequency Range. *IEEE Trans. Antennas Propag.* **2018**, *66*, 2828–2843.
80. Pozar, D.M. *Microwave Engineering: Theory and Techniques*; John Wiley & sons, 2021.
81. Konstantinidis, K.; Feresidis, A.P.; Hall, P.S. Dual-slot feeding technique for broadband Fabry–Perot cavity antennas. *IET Microw., Antennas Propag.* **2015**, *9*, 861–866.
82. Foster, R.M. A reactance theorem. *Bell Sys. Techn. J.* **1924**, *3*, 259–267.
83. Baccarelli, P.; Burghignoli, P.; Di Nallo, C.; Frezza, F.; Galli, A.; Lampariello, P.; Ruggieri, G. Full-wave analysis of printed leaky-wave phased arrays. *Int. J. RF Microw. Comput.-Aided Eng.* **2002**, *12*, 272–287.
84. Giusti, F.; Chen, Q.; Mesa, F.; Albani, M.; Quevedo-Teruel, O. Efficient Bloch analysis of general periodic structures with a linearized multimodal transfer-matrix approach. *IEEE Trans. Antennas Propag.* **2022**, *70*, 5555–5562.
85. Valerio, G.; Paulotto, S.; Baccarelli, P.; Burghignoli, P.; Galli, A. Accurate Bloch analysis of 1-D periodic lines through the simulation of truncated structures. *IEEE Trans. Antennas Propag.* **2011**, *59*, 2188–2195.
86. Mesa, F.; Valerio, G.; Rodríguez-Berral, R.; Quevedo-Teruel, O. Simulation-Assisted Efficient Computation of the Dispersion Diagram of Periodic Structures: A comprehensive overview with applications to filters, leaky-wave antennas and metasurfaces. *IEEE Antennas Propag. Mag.* **2021**, *63*, 33–45. <https://doi.org/10.1109/MAP.2020.3003210>.
87. Apaydin, N.; Zhang, L.; Sertel, K.; Volakis, J.L. Experimental Validation of Frozen Modes Guided on Printed Coupled Transmission Lines. *IEEE Trans. Microw. Theory Techn.* **2012**, *60*, 1513–1519. <https://doi.org/10.1109/TMTT.2012.2192746>.
88. Negri, E.; Giusti, F.; Fuscaldo, W.; Burghignoli, P.; Martini, E.; Galli, A. Generation of a Long-Nondiffractive-Range Leaky-Wave Bessel Beam through an Open-Stopband Mitigation Technique. In Proceedings of the

- International Symposium on Antennas and Propagation (ISAP) 2024, Accepted for Publication, 2024; pp. 1–2.
89. Liu, J.; Zhou, W.; Long, Y. A Simple Technique for Open-Stopband Suppression in Periodic Leaky-Wave Antennas Using Two Nonidentical Elements Per Unit Cell. *IEEE Trans. Antennas Propag.* **2018**, *66*, 2741–2751. <https://doi.org/10.1109/TAP.2018.2819701>.
 90. Al-Bassam, A.; Otto, S.; Heberling, D.; Caloz, C. Broadside Dual-Channel Orthogonal-Polarization Radiation Using a Double-Asymmetric Periodic Leaky-Wave Antenna. *IEEE Trans. Antennas Propag.* **2017**, *65*, 2855–2864. <https://doi.org/10.1109/TAP.2017.2691467>.

Disclaimer/Publisher’s Note: The statements, opinions and data contained in all publications are solely those of the individual author(s) and contributor(s) and not of MDPI and/or the editor(s). MDPI and/or the editor(s) disclaim responsibility for any injury to people or property resulting from any ideas, methods, instructions or products referred to in the content.